Angle Droop Design for Grid-Forming Inverters Considering Impacts of Virtual Impedance Control

Le Kong
Department of Electrical Engineering and Computer Science
The University of Tennessee, Knoxville
Knoxville, USA
lkong4@vols.utk.edu

Yaosuo Xue
Energy Science and Technology Directorate
Oak Ridge National Laboratory
Knoxville, USA
xuey@ornl.gov

Liang Qiao
Department of Electrical Engineering and Computer Science
The University of Tennessee, Knoxville
Knoxville, USA
lqiao1@vols.utk.edu

Fei (Fred) Wang[1,2]
[1]*The University of Tennessee, Knoxville*
[2]*Oak Ridge National Laboratory*
Knoxville, USA
fred.wang@utk.edu

***Abstract*—Grid-forming inverters (GFMs) based on active power-frequency droop control and reactive power-voltage droop control have been developed in recent years, which can generate voltage and frequency references for islanded power systems or microgrids to improve system-wide synchronization and power-sharing capability. It is known that the control delays in GFMs may cause system harmonic instability. To eliminate this issue, virtual impedance techniques are normally adopted. This paper gives a comprehensive examination of the impacts of virtual impedance control block Z_v in GFMs on system stability. It is revealed that although Z_v is effective in eliminating system harmonic stability, it may ruin system synchronization stability as a side effect. To compensate for the negative impacts caused by Z_v, an active power-angle control block is added into the conventional droop control. Design criteria are also proposed accordingly to ensure system stability over the entire frequency range. Simulations and experimental testing are conducted to validate the analysis and the proposed design guidelines. It can be concluded that the Z_v control-caused grid-synchronization instability issues can be eliminated with an appropriate active power-angle droop design.**

Keywords—Angle droop control, grid forming inverter, harmonic instability, synchronous stability, virtual impedance control

I. INTRODUCTION

Different types of voltage-controlled converters, which are termed as grid-forming inverters (GFMs), have been developed to generate system frequency and voltage autonomously, including droop control, virtual synchronous control, virtual oscillator control, etc.[1-4]. Among them, the most well-developed grid-forming approach is the droop control, which was first proposed in the 1990s [5]. It enables multiple GFMs to share and deliver desired active and reactive power into the system through local control in a stable manner. A typical droop control includes an active power-frequency (*P-f*) droop and a reactive power-voltage (*Q-v*) droop. The general circuit diagram of the conventional droop-control based GFM is shown in Fig. 1 [3, 4, 6]. The outer power loop is to provide a well-defined voltage reference with proper amplitude and phase. Additionally, the inner voltage-current control loops are designed to regulate the output voltage, provide damping for the *LC* resonance, and limit the converter overcurrent. These control blocks can be implemented in either $\alpha\beta$ or *dq* frames. The controllers used in this paper are implemented in $\alpha\beta$ frame.

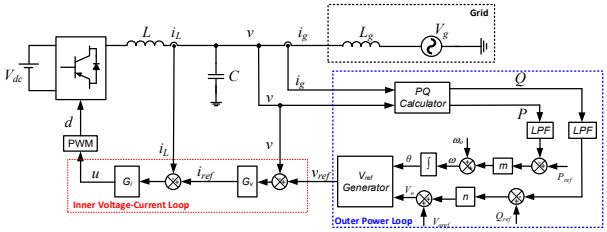

Fig. 1. Circuit diagrams of typical droop-control based GFMs.

To study the dynamic characteristics of droop-control-based GFMs and their impacts on system stability, both impedance-based Nyquist stability criterion and passivity-based stability analysis approaches have been adopted in the literature [7-10]. Generally speaking, the impacts of droop-controlled GFMs on system stability can be roughly categorized into two types: grid-synchronization stability (in the low-frequency range near fundamental frequency) and harmonic stability (in the high-frequency range about several hundred Hz to several kHz). For the analysis of system synchronization stability, the Nyquist stability criterion with a full-order complex-value-based output impedance has been used [4, 8, 9]. It has been pointed out that GFMs tend to induce sub-synchronous oscillations (SSO) under stringent grid conditions because the smaller the grid impedance is, the larger damping will be needed, which means that the smaller the *p-f* gain *m* will be allowed. Hence, to ensure stable operation of systems in the low-frequency range, the droop gains (*m* and *n*) in the outer power loop should be designed according to the grid conditions. For the analysis of system harmonic instability issues, the passivity-based stability criterion with the inverter output impedance has been used to identify the root causes. And it has been found that converter control delays will cause a non-passive region in the output impedance at high frequencies, within which the negative damping will be introduced to the current control and destabilize the system. Accordingly, passivity-based control solutions have been proposed, such as adding both virtual impedance control function Z_v and the voltage feedforward control function H_v to the inner voltage-current loop as shown in Fig. 2 [7, 10]. With these two blocks Z_v and H_v, the inverter passivity can be guaranteed up to Nyquist frequency. Therefore, the system harmonic instability issues caused by converter control delays can be eliminated regardless of the strength of the grid impedance.

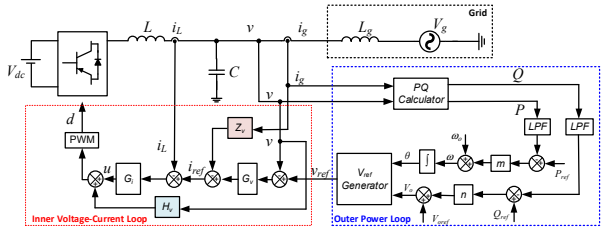

Fig. 2 . Circuit diagrams of typical droop-control based GFMs with Z_v and H_v control blocks [7].

However, it is found in this paper that the Z_v block, which is initially designed for harmonic stability enhancement, might bring sub-synchronous oscillations into the system. To have a better understanding of the Z_v impact on system stability, fundamental mechanisms of Z_v control blocks are analyzed first in Section II. Based on the analysis results, an active power-angle droop control block is added to the conventional droop control loop and the design guidelines are also proposed in Section III, to eliminate the negative impacts caused by Z_v on grid-synchronization stability and to keep the positive impacts on harmonic stability at the same time. Simulation and experimental results are presented in Section IV to validate the effectiveness of the proposed design criteria for the active power-angle droop gain. Section V concludes the paper.

II. Impacts of Z_V Control on System Stability

A. Positive Impacts of Z_v on System Harmonic Stability – A Review

Passivity-oriented design is an effective stability enhancement approach and such studies have also been applied for grid forming inverters (GFMs) as in [7, 10, 11]. First, to analyze the passivity of GFMs, the single-input-single-output (SISO) output impedance model $Z_{ov}(s)$ needs to be derived. Equation (1) shows the output impedance model $Z_{ov}(s)$, where Z_{ol} is the open-loop output impedance, G_{ui}, G_{uv}, and G_{ii} are the transfer functions from converter-side voltage to inductor current, converter-side voltage to output voltage, and grid-side current to inductor current separately, G_i is the current controller, G_v is the voltage controller, and G_d is the system control delay which is typically 1.5 times of the converter switching period. Note that the SISO impedance model introduced here only intends for harmonic stability analysis, and low-frequency characteristics are ignored. For more details about the model derivation, one can refer to [10].

$$Z_{ov}(s) = \frac{Z_{ol}(1 + G_{ui}G_iG_d) + G_{uv}G_dG_iG_{ii}}{1 + G_{ui}G_iG_d + G_{uv}G_vG_iG_d} \quad (1)$$

The Bode diagram of the impedance model $Z_{ov}(s)$ is obtained as shown in Fig. 3. From the plot, it is seen that there is a high-frequency non-passive region (HF-NPR), i.e., phase angle exceeds the range of [-90°, 90°], which is identified to be caused by the converter control delays. In the HF-NPR, harmonics instability issues might happen when the grid side impedance is changed.

To eliminate this HF-NPR, a linear voltage controller with virtual impedance Z_v and voltage decouple control H_v can be added in the inner voltage-current loop. With the Z_v and H_v control blocks, the original output impedance $Z_{ov}(s)$ is modified to be $Z_{ov\_c}(s)$ as given in (2).

$$Z_{ov\_c}(s) = \frac{Z_{ol}(1 + G_{ui}G_iG_d) + G_{uv}G_dG_i(G_{ii} + Z_v)}{1 + G_{ui}G_iG_d + G_{uv}G_d(G_vG_i - H_v)} \quad (2)$$

Similarly, the Bode diagram of $Z_{ov\_c}(s)$ is given in Fig. 3. It is seen that the HF-NPR below Nyquist frequency can be removed with the help of the Z_v and H_v compensation blocks.

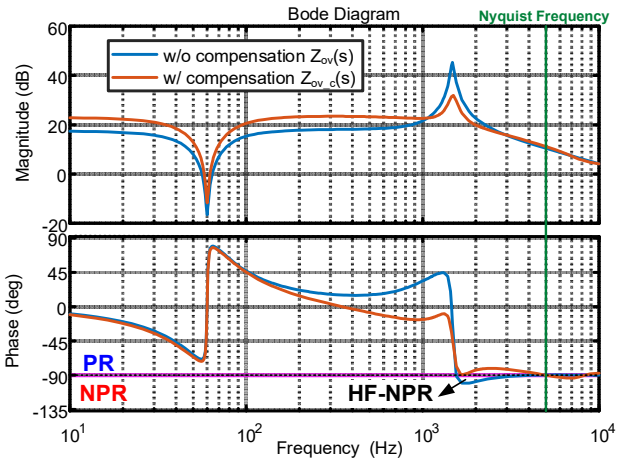

Fig. 3. Bode diagrams of impedance model of GFMs w/o and w/ passivity compensation blocks (Z_v and H_v).

Note that both Z_v and H_v need to be added to achieve the passivation of the GFMs up to the Nyquist frequency. If with H_v only, the system stability margin could be improved, but system harmonic instability issues cannot be solved thoroughly since the inverter still has some non-passive regions. Once the grid condition changes, harmonic instability might still happen. One can see more case studies later in Section II-B.

B. Negative Impacts of Z_v on Grid-Synchronization Stability

1) Simulation investigation

To see the negative impacts of Z_v block on system synchronization stability, a simulation testing platform is built in MATLAB/Simulink following the circuit structure as shown in Fig. 2 with the parameters listed in Table I.

Table I. Circuit and control parameters in simulation testing

Variables	Value	Variables	Value
Grid voltage RMS value V_g	190 V	Fundamental frequency f_0	60 Hz
GFM voltage RMS value V_o	190 V	Switching frequency f_{sw}	10 kHz
LC filter capacitance L, C	2 mH, 10 μF	Power references P_0 , Q_0	2 kW, 0 Var
Grid impedance L_g	8 mH / 6 mH / 4 mH / 2 mH	Short circuit ratio SCR	6 / 8 / 12 / 24
Control delay T_d	$1.5/f_{sw}$	Current control G_i	8
Voltage control G_v	$50 + \frac{0.01s}{s^2 + 7.5398s + 142122}$		

In these cases, the grid impedance L_g range from 8 mH to 2 mH (i.e., SCR from 6 to 24) to emulate weak grid and strong grid conditions. The p-f droop gain m and Q-v droop gain n are then designed respectively based on the grid conditions using Nyquist stability criterion with assuming the converter

control delay is ideally small enough, i.e., $T_d = 0.5T_{sw}$. This guarantees that under ideal situations, there are no high-frequency (HF) harmonics and no low-frequency (LF) SSO. Then, a larger control delay ($1.5T_{sw}$), which is also a typical and practical value in most cases, is taken into considerations.

Simulations with different control structures (CI: w/o Z_v and w/o H_v, CII: w/o Z_v and w/ H_v, CIII: w/ Z_v and w/ H_v) are investigated. For example, when SCR = 8, the frequency droop gain is designed as $2\%\omega_0/P_0$ and the voltage droop gain is $10\%V_0/P_0$ (for simplicity, only the ratio will be given in the following text), and the simulation results show that with CI, there will be high-frequency harmonic instability issues with the harmonics component to be around 1.5 kHz as shown in Fig. 4. If there is no Z_v, but H_v is added, that is with CII, the system is stable as shown in Fig. 5. While with CIII, high-frequency harmonics can be eliminated, but low-frequency SSO (57.6 Hz and 62.4 Hz) will be introduced into the system as shown in Fig. 6.

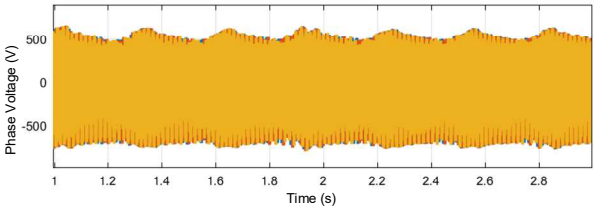

(a)

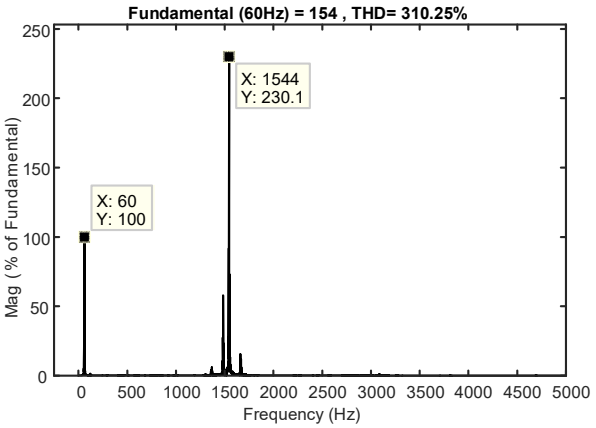

(b)

Fig. 4. Simulation results of harmonic instability issues with CI when SCR = 8 (m = 2% and n = 10%): (a) simulation waveforms of phase voltage and (b) FFT analysis of phase voltage.

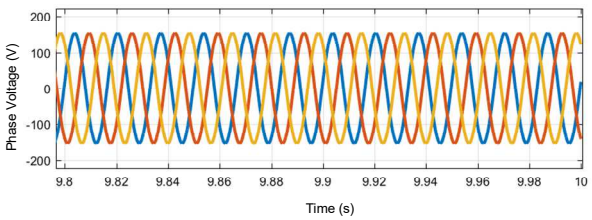

Fig. 5. Simulation waveforms of phase voltage in a stable system with CII when SCR = 8 (m = 2% and n = 10%).

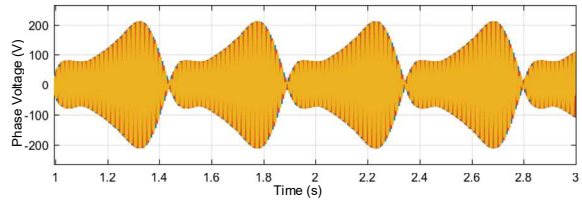

(a)

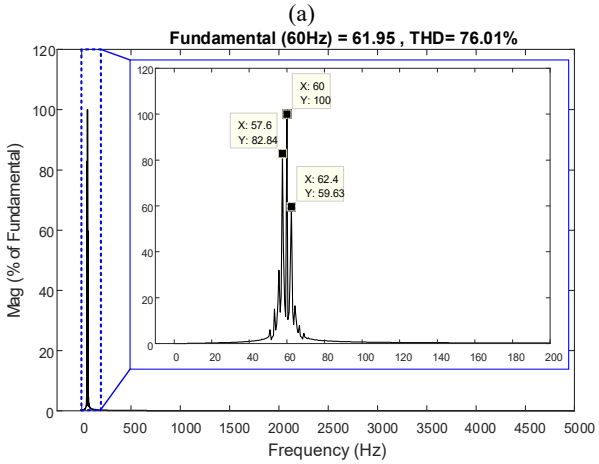

(b)

Fig. 6. Simulation results of SSO issues with CIII when SCR = 8 (m = 2% and n = 10%): (a) simulation waveforms of phase voltage and (b) FFT analysis of phase voltage.

More cases under different grid conditions are summarized in Table II, where HF Harmonics refer to the unstable phenomena similar to that in Fig. 4 and LF SSO refers to instabilities similar to that in Fig. 6.

Table II. Simulation results under different grid conditions with different control structures

Grid Conditions	CI	CII	CIII
SCR = 6 (m = 2% & n = 10%)	Stable	Stable	Stable
SCR = 8 (m = 2% & n = 10%)	HF Harmonics	Stable	LF SSO
SCR = 12 (m = 0.5% & n = 2.5%)	HF Harmonics	Stable	LF SSO
SCR = 24 (m = 0.2% & n = 1%)	HF Harmonics	HF Harmonics	LF SSO

Several findings could be summarized from Table II. First, it is seen that without the passivity compensation blocks (CI: w/o Z_v and w/o H_v), the system will have high-frequency harmonic instability issues when SCR is large (SCR = 8, 12, and 24). Second, with H_v only (CII), system stability can be improved (stable under SCR = 8 or 12), but it still has harmonic instability issues when SCR = 24. Third, with both Z_v and H_v compensation blocks (CIII), there will be no HF harmonic issues in the system; however, LF SSO will be introduced instead. Therefore, it can be concluded that the Z_v compensation block can help with system high-frequency stability, but it may negatively impact system low-frequency resonance as well.

2) Theoretical analysis

To analyze the fundamental mechanism of Z_v impacts on system synchronization stability, an equivalent virtual impedance Z_{veq} is obtained first by moving the Z_v block to the

input side of the voltage controller G_v as shown in Fig. 7, which can be expressed as in (3) with an equivalent frequency-dependent virtual resistance R_{veq} and a virtual reactance X_{veq}. The values of the equivalent virtual impedance in this study are calculated as shown in Fig. 8. It can be seen that the equivalent R_{veq} is large enough ($R_{veq} >> X_{veq}$) in both LF and HF ranges to provide enough damping for the system, but near the fundamental frequency f_{fund} (shaded area in Fig. 8), the R_{veq} is almost 0 which means there is no resistive damping provided for the system in this frequency range.

$$Z_{veq}(\omega) = Z_v/G_v(j\omega) = R_{veq}(\omega) + jX_{veq}(\omega) \tag{3}$$

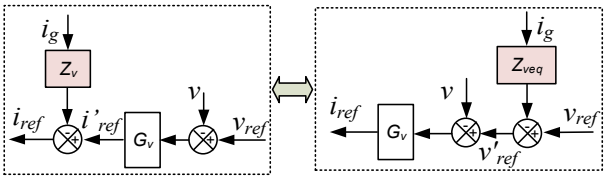

Fig. 7. Equivalent virtual impedance in the control diagrams.

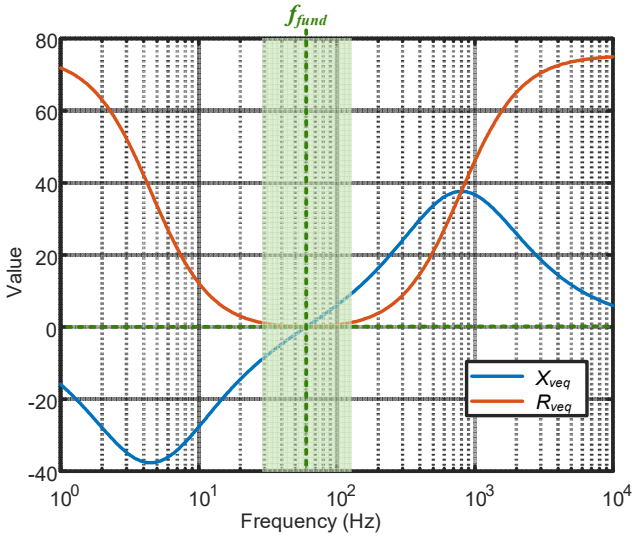

Fig. 8. Frequency-dependent values of equivalent impedance.

Then, assuming the inner voltage-current loop to be 1 since LF SSO is under investigation, the system equates to a grid-connected voltage source with Z_{veq} as shown in Fig. 9. This virtual impedance Z_{veq} will reduce the output voltage reference proportionally to the output current as shown in (4). Accordingly, the power flow S can be calculated as (5). Based on (4) and (5), the equations about magnitude and phase angle of the reference voltage v'_{ref} and output voltage v are obtained as (6) and (7) [12,13].

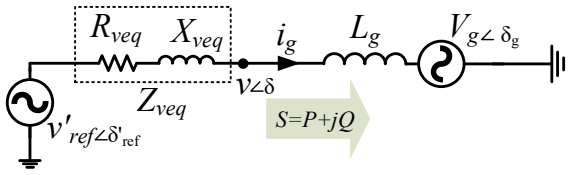

Fig. 9. Equivalent virtual impedance in the entire system.

$$V'_{ref} = V_{ref} - Z_{veq} i_g \tag{4}$$

$$S = P + jQ = v\angle\delta\left(\frac{v'_{ref}\angle\delta'_{ref} - v\angle\delta}{R_{veq} + jX_{veq}}\right)^* \tag{5}$$

$$\Delta v = v'_{ref} - v \cong \frac{R_{veq}P + X_{veq}Q}{v} \tag{6}$$

$$\delta_v = \delta'_{ref} - \delta \cong \frac{X_{veq}P - R_{veq}Q}{v'_{ref}v} \tag{7}$$

Assume v'_{ref} and v are equal to V_o for simplicity, which is true for most conditions since the voltage magnitude should be limited within a narrow range. Besides, it is seen from Fig. 8 that the calculated value of R_{veq} is almost 0 around f_{fund}. Equations (8) and (9) can then be obtained. It is found that in the P-f control loop, the virtual impedance control Z_v adds an equivalent power-angle droop gain m_e, and in the Q-v control loop, Z_v adds an equivalent voltage droop gain n_e. The Q-v loop dynamics expressed in (9) can be ignored as long as $n + n_e$ is larger than 0 since it has little impact on system stability [9,14]. While the Z_v-induced m_e as expressed in (8) turns out to be the culprit for the LF SSO issues in the system as analyzed below.

$$\omega \approx \omega_o - mP_{LPF} - m_e(f)\frac{dP}{dt} \tag{8}$$

$$V_o \approx V_{ref} - nQ_{LPF} - n_e(f)Q \tag{9}$$

where, $m_e(f) = \frac{X_{veq}(f)}{V_o^2}$ and $n_e(f) = \frac{X_{veq}(f)}{V_o}$.

First, small-signal stability analysis on the active power loop is conducted with the linearized model derived in (10) based on the equivalent circuit as shown in Fig. 10 [12,13], where the cut-off frequency of the low-pass filter ω_{LPF} is 2π rad/s. Based on the characteristics equation of (10), it can be concluded that the Z_v block does not affect the small-signal stability of the system since all the eigenvalues locate in the left half-plane (LHP).

$$\Delta P = \frac{G(s + \omega_{LPF})}{(1 + m_eG)s^2 + \omega_{LPF}(1 + m_eG)s + \omega_{LPF}mG}(\Delta\omega - \Delta\omega_g) \tag{10}$$

where, $G = \partial P/\partial\delta_l$, $\delta_l = \delta - \delta_g$.

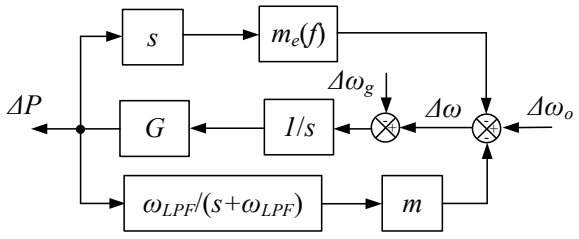

Fig. 10. Small-signal model of active power loop considering virtual impedance impact.

Second, the analysis is extended to the transient stability of the system. The swing equation which describes the behaviors of the active power loop can be derived as shown in (11), where H is the inertia time constant, and D is the damping coefficient [14]. It is seen that the equivalent m_e term will add m_eP_{max} on both system inertia and damping. As seen

from Fig. 8, X_{veq} is a negative value below f_{fund} which means m_e will also be negative below f_{fund}. Though it is difficult to quantify the damping and inertia value and to draw the phase portrait for the analysis of system stability since m_e is a variable frequency-dependent value, the negative impacts can still be observed from Fig. 11, where H_0 and D_0 are the original system inertia and damping without Z_v, and H and D are the ones considering Z_v impacts. Hence, it can be inferred that the system stability will be affected since a system with less damping is more likely to have LF SSO issues as shown in Table II.

$$H\ddot{\delta} = P_{ref} - P_{max}sin\delta - D\dot{\delta} \tag{11}$$

where,

$$H = \frac{1 + m_e P_{max}}{\omega_{LPF} m} \tag{12}$$

$$D = \frac{1 + m_e P_{max}}{m} \tag{13}$$

$$P_{max} = \frac{V_o^2}{X_g} \tag{14}$$

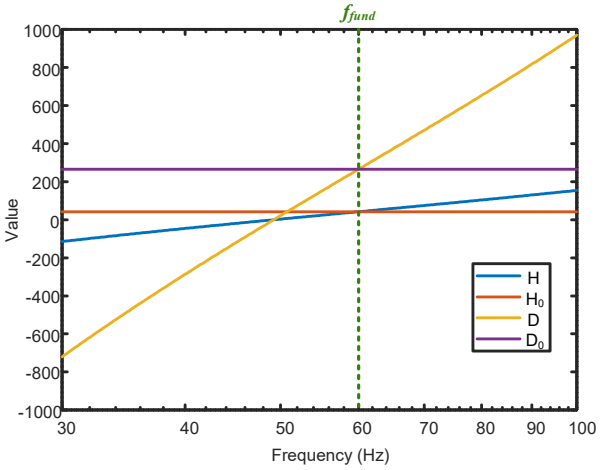

Fig. 11. Impacts of Z_v on system inertia and damping constant.

Finally, it can be concluded that the virtual impedance control block, which is intended to eliminate the system harmonic instability issues, might reduce the system damping near f_{fund} and cause LF SSO issues in the system. Note that although the analysis method introduced here is only valid near f_{fund} (30 Hz to 100 Hz) since R_{veq} can only be assumed to be 0 in this region, it is already good enough for the SSO stability analysis. In addition, in the LF or HF ranges, R_{veq} is large enough to provide damping for the system and can help to maintain system stability.

III. Design Guidelines for Modified Outer Power Loop Considering Z_V Impacts

Based on the simulation studies and theoretical analysis above, a direct solution can be proposed to eliminate the negative damping impact of Z_v on active power droop control, that is adding corresponding droop compensation gains to compensate the Z_v induced negative value of the equivalent angle droop gain $m_e(f)$ and voltage droop gain $n_e(f)$. Therefore, an angle droop gain k_1 (rad/W) is added to the active power droop loop, and a voltage droop gain k_2 (V/Var) is added into the reactive power droop loop as shown in Fig. 12. This modified outer power loop (i.e., conventional droop plus angle droop) is not a new topology and has been proven to be able to improve the converter power-sharing capability in [15]. But in this paper, the modified droop controls are mainly designed for the consideration of the impacts of Z_v so that both LF SSO issues and harmonic instability issues can be eliminated. The design criteria for the droop gains k_1 and k_2 can be obtained as shown below.

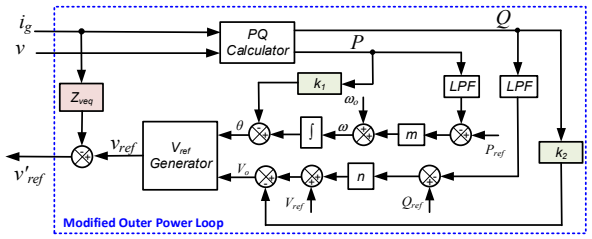

Fig. 12. Control function blocks of the modified outer power loop with compensation gains.

To eliminate the low-frequency impacts caused by Z_v on the swing equation, the power-angle droop gains considering both k_1 and Z_v induced $m_e(f)$ should meet the criteria that is $m_e(f) + k_1 > 0$ (Criterion 1) to fully compensate for the negative damping impacts of Z_v within the studied frequency range. Note that similar to the analysis in (10), adding k_1 will not introduce any right half plane poles in the system from the aspects of system small-signal stability.

Based on Criteria 1, k_1 should be large enough so that it would be effective for the elimination of low-frequency resonance with good system dynamics. However, k_1 cannot be designed to be too large either in order to keep the passivity of the GFM at high frequency. Based on the Bode plots shown in Fig. 13, when k_1 is small (1.8×10^{-5} or 3×10^{-5}), the inverter output impedances stay unchanged compared with baseline impedance when $k_1 = 0$. However, if increasing k_1 to be 7.5×10^{-5}, the inverter will show an HF-NPR as the phase value indicates. Therefore, to maintain inverter passivity compensated by Z_v block, R_{veq} should dominate the Z_{veq} characteristics at high frequencies, i.e., $R_{veq} >> X_{veq} + k_1 \times V_{nom}^2$ (Criteria 2), to avoid the impacts of k_1 on inverter passivity for system harmonic stability.

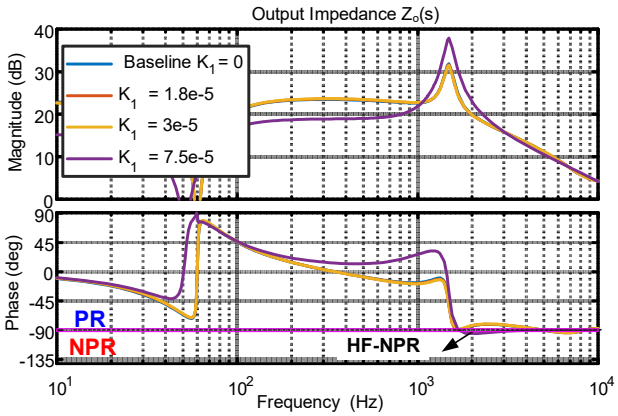

Fig. 13. Passivity enhanced $Z_o(s)$ with different k_1.

Additionally, if considering the reactive power dynamics, the sum of the Q-v droop gains, including original gain n, Z_v induced $n_e(f)$, and k_2, should be larger than 0, i.e., $n + n_e + k_2 > 0$ (Criterion 3). As mentioned in Section II-B, active power droop is the dominant loop for system transition dynamics, therefore, k_1 is the key to system stability and k_2 is less

important. For simplicity, k_2 can be designed as $V_{nom} \times k_1$ first and then checked with Criterion 3.

IV. Simulation and Experimental Validations

A. Simulation Validation

1) System Stability Enhancement with Angle Droop

To eliminate the LF SSO of the cases studied in Table II with CIII, droop compensations are implemented at $t = 6$ s in the simulations. For SCR = 8, 12, and 24, k_1 is designed to be 6×10^{-5}. It can be seen from Fig. 14, by adding proper angle droop control, the LF SSO issues can all be eliminated.

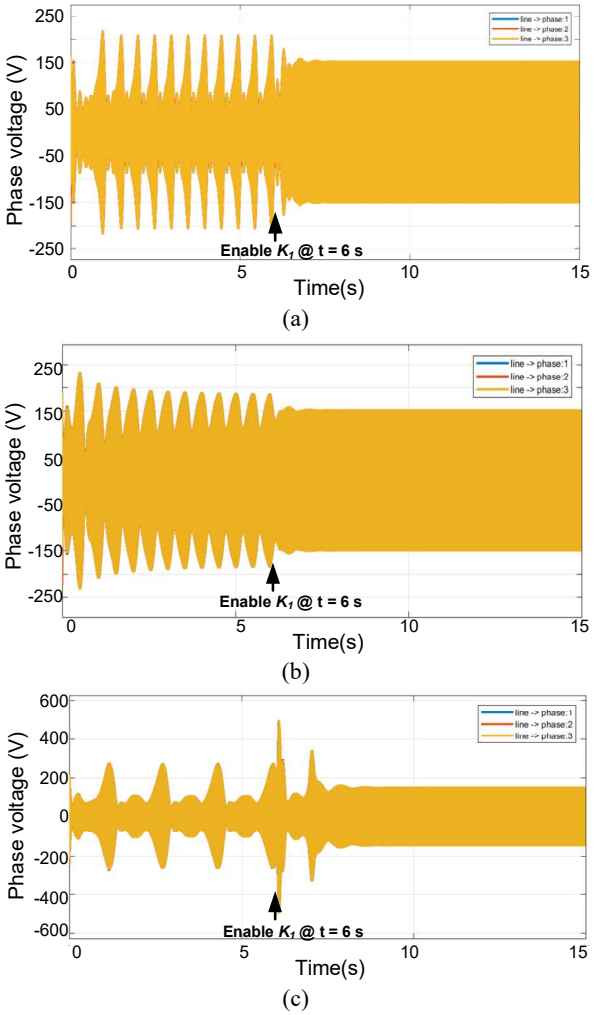

Fig. 14. Simulation results under different cases: (a) SCR = 8 (b) SCR = 12, and (c) SCR = 24.

2) Impacts of Different Modified Droop Gain Values on System Stability

Effects of the k_1 values on system performance have also been investigated under SCR = 8 as shown in Fig. 15. If k_1 is too small, the low-frequency resonance will not be eliminated as in Fig. 15 (a). Within the proper design range, the system will be stabilized, and a larger k_1 will provide better dynamics as shown in Fig. 15 (b) and Fig. 15 (c). While if k_1 is too large, inverter passivity will be affected and harmonic instability will happen as shown in the zoom-in view of Fig. 15 (d).

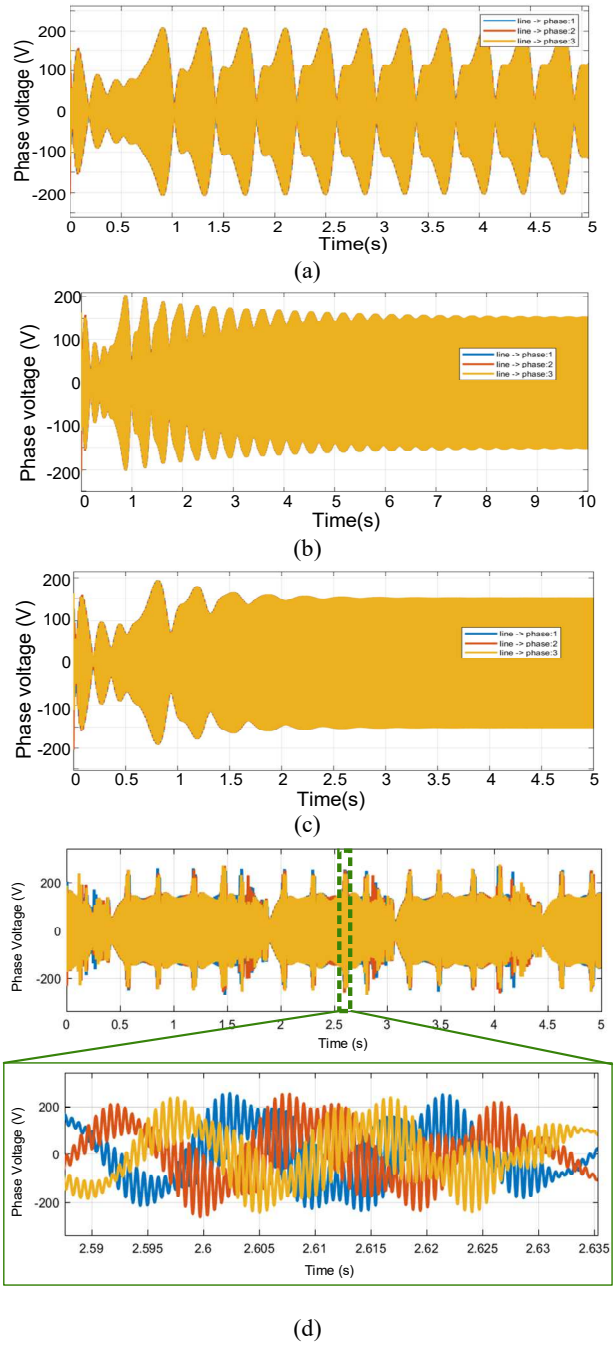

Fig. 15. Simulation results with different k_1 under SCR = 8: (a) 1.2×10^{-5}, (b) 1.8×10^{-5}, (c) 3×10^{-5}, and (d) 3×10^{-4}.

B. Experimental Validation

To further validate the effectiveness of the angle droop gain on the compensation of the negative impact of Z_v on system LF stability, an experimental platform is built as shown in Fig. 16. Two converters are used to mimic the circuit connections in Fig. 2. The first converter is a grid emulator using open-loop control with grid impedance (L_g = 3.6 mH), and the second converter is the droop-controlled GFM with output filters (L = 2.4 mH and C_f = 10 µF). The reference powers in the test are 600 W and 0 Var. In addition, the reference output voltage and grid voltage is 50 $V_{LL,rms}$. The control parameters are the same as those in Table I.

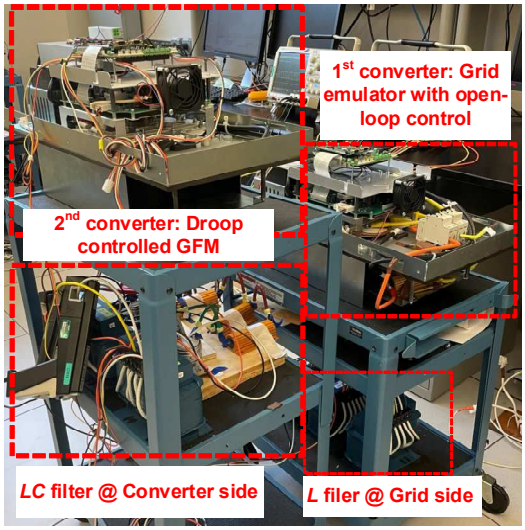

Fig. 16. Experimental setup.

The impact of Z_v on system stability is investigated first. From Fig. 17(a), it can be seen that if the controller is implemented with CI (i.e., no Z_v and no H_v), there will be HF harmonic issues on the output voltage. If the controller is implemented with CIII (i.e., with Z_v and with H_v), it is seen from the full view of Fig. 17(b) that there will be LF SSO, while there is no HF harmonics as seen from the zoom-in view of Fig. 17(b). Note that the controller implemented with CII (i.e., no Z_v but with H_v) will not be shown here since the system is stable.

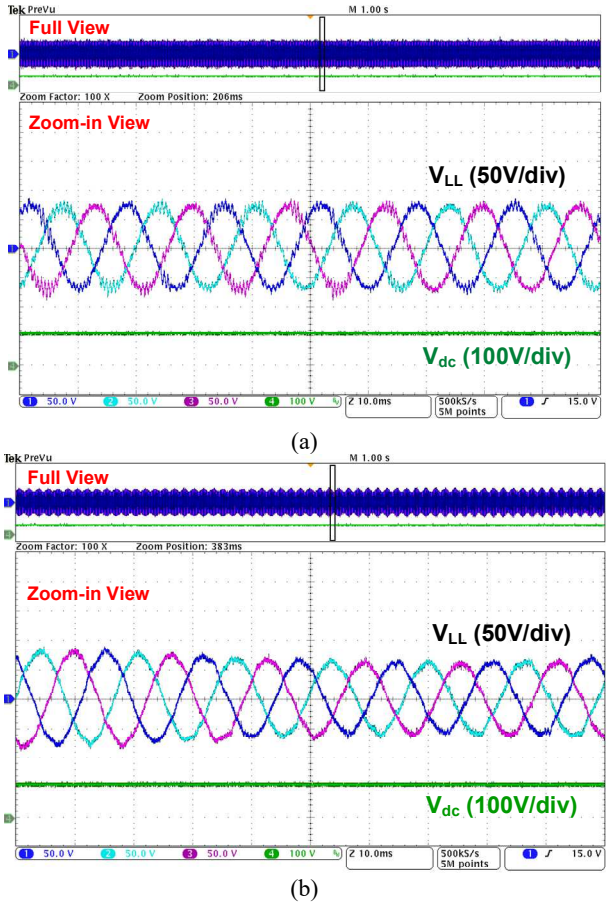

Fig. 17. Impacts of Z_v on system stability: (a) with CI and (b) with CIII.

The LF SSO caused by the negative impact of Z_v can be eliminated by adding active power-angle droop control as shown in Fig. 18.

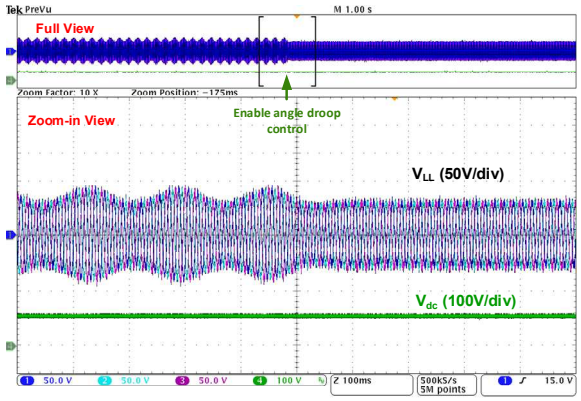

Fig. 18. Elimination of Z_v–induced LF SSO with angle droop control.

V. Conclusions

This paper analyzes both the positive and negative impacts of virtual impedance control block Z_v on system stability. With Z_v block, the inverter can be designed to be passive at high frequency, and therefore, the HF harmonic instability issues can be eliminated for all grid conditions. However, the Z_v block will also affect system LF stability by reducing the inertia and damping of the system. Therefore, to eliminate the negative impact caused by Z_v, an angle droop control block is added to the *P-f* droop control, and the design criteria for the gains are proposed accordingly. Simulations and experimental results are also given to validate the effectiveness of the angle droop control in eliminating negative impacts of Z_v.

Notice of Copyright

Acknowledgment

This material is based upon work supported by the US Department of Energy, Office of Electricity, Advanced Grid Modeling Program under contract DE-AC05-00OR22725. This work also made use of Engineering Research Center Shared Facilities provided by the Engineering Research Center Program of the National Science Foundation and the Department of Energy under NSF Award Number EEC1041877 and the CURENT Industry Partnership Program.

References

[1] Q. Zhong, "Power-Electronics-Enabled Autonomous Power Systems: Architecture and Technical Routes," *IEEE Transactions on Industrial Electronics,* vol. 64, no. 7, pp. 5907-5918, 2017.

[2] G. Seo, M. Colombino, I. Subotic, B. Johnson, D. Groß, and F. Dörfler, "Dispatchable Virtual Oscillator Control for Decentralized Inverter-dominated Power Systems: Analysis and Experiments," in *IEEE Applied Power Electronics Conference and Exposition (APEC)*, 2019, pp. 561-566.

[3] M. A. Awal, H. Yu, S. Lukic, and I. Husain, "Droop and Oscillator Based Grid-Forming Converter Controls: A Comparative Performance Analysis,", *Frontiers in Energy Research,* Original Research vol. 8, no. 168, 2020.

[4] W. Du *et al.*, "A Comparative Study of Two Widely Used Grid-Forming Droop Controls on Microgrid Small-Signal Stability," *IEEE Journal of Emerging and Selected Topics in Power Electronics,* vol. 8, no. 2, pp. 963-975, 2020.

[5] M. C. Chandorkar, D. M. Divan, and R. Adapa, "Control of Parallel Connected Inverters in Standalone AC Supply Systems," *IEEE Transactions on Industry Applications,* vol. 29, no. 1, pp. 136-143, 1993.

[6] Y. Li, Y. Gu, Y. Zhu, A. J. Ferre, X. Xiang, and T. C. Green, "Impedance Circuit Model of Grid-Forming Inverter: Visualizing Control Algorithms as Circuit Elements," *IEEE Transactions on Power Electronics,* pp. 1-1, 2020.

[7] Y. Liao, X. Wang, and F. Blaabjerg, "Passivity-Based Analysis and Design of Linear Voltage Controllers For Voltage-Source Converters," *IEEE Open Journal of the Industrial Electronics Society,* vol. 1, pp. 114-126, 2020.

[8] X. Wang, M. G. Taul, H. Wu, Y. Liao, F. Blaabjerg, and L. Harnefors, "Grid-Synchronization Stability of Converter-Based Resources An Overview," *IEEE Open Journal of Industry Applications,* pp. 1-1, 2020.

[9] Y. Liao, X. Wang, F. Liu, K. Xin, and Y. Liu, "Sub-Synchronous Control Interaction in Grid-Forming VSCs with Droop Control," in *IEEE Workshop on the Electronic Grid (eGRID)*, 2019, pp. 1-6.

[10] Y. Liao and X. Wang, "Passivity Analysis and Enhancement of Voltage Control for Voltage-Source Converters," in *IEEE Energy Conversion Congress and Exposition (ECCE)*, 2019, pp. 5424-5429.

[11] H. Yu, M. A. Awal, H. Tu, Y. Du, S. Lukic, and I. Husain, "Passivity-Oriented Discrete-Time Voltage Controller Design for Grid-Forming Inverters," in *IEEE Energy Conversion Congress and Exposition (ECCE)*, 2019, pp. 469-475.

[12] Y. Sun, X. Hou, J. Yang, H. Han, M. Su, and J. M. Guerrero, "New Perspectives on Droop Control in AC Microgrid," *IEEE Transactions on Industrial Electronics,* vol. 64, no. 7, pp. 5741-5745, 2017.

[13] G. Yajuan, W. Weiyang, G. Xiaoqiang, and G. Herong, "An Improved Droop Controller for Grid-Connected Voltage Source Inverter in Microgrid," in *International Symposium on Power Electronics for Distributed Generation Systems*, 2010, pp. 823-828.

[14] X. Fu, J. Sun, M. Huang, Z. Tian, H. Yan, H. Iu, P. Hu, and X. Zha, "Large-Signal Stability of Grid-Forming and Grid-Following Controls in Voltage Source Converter: A Comparative Study," *IEEE Transactions on Power Electronics,* vol. 36, no. 7, pp. 7832-7840, 2021.

[15] R. Majumder, G. Ledwich, A. Ghosh, S. Chakrabarti, and F. Zare, "Droop Control of Converter-Interfaced Microsources in Rural Distributed Generation," *IEEE Transactions on Power Delivery,* vol. 25, no. 4, pp. 2768-2778, 2010.